Electronic Supplementary Information

$NaNi_{0.5}Mn_{0.5}Sn_xO_2$ Cathode with Anti Structural Deformation Enhancing Long Lifespan and Super Power for Sodium Ion Battery

*Yiming Meng, †[a] Juan An, †[a] Lei Chen, [b] Guorong Chen, *[a] Liyi Shi, [a] Mi Lu [c] and Dengsong Zhang *[a]*

[a] Department of Chemistry, Research Center of Nano Science and Technology, College of Sciences, Shanghai University, Shanghai 200444, China

[b] College of Engineering, Zhejiang A & F University, 666 Wusu Street, Hangzhou 311300, China

[c] School of Materials Science and Engineering, Xiamen University of Technology, Xiamen, China, 361024

*Correspondence: chengr@t.shu.edu.cn

*Correspondence: dszhang@shu.edu.cn

† Yiming Meng and Juan An contributed equally to this work.

Experimental section

Materials synthesis: The O3-$NaNi_{0.5}Mn_{0.5}Sn_xO_2$ (x = 0, 0.01, 0.03 and 0.05) materials were synthesized by sol-gel method. The stoichiometric mixture of sodium acetate (Alfa Aesar, 99%), manganese (II) acetate (Alfa Aesar, 98%) and nickel (II) acetate (Alfa Aesar, 98%) are dissolved in deionized water forming a uniform solution. Then, the solution was stirred during heating at 80°C for 5 hours to get a green gel. After that, the gel was dried in an oven at 120°C for 24 hours and a precursor of $NaNi_{0.5}Mn_{0.5}O_2$ was obtained. The solid precursor was ground uniformly, placed in a corundum crucible and calcined in a muffle furnace at 1000° C for 12 h, quenched to room temperature, and then subjected to secondary calcination to obtain a cathode material having higher purity. Transfer the black $NaNi_{0.5}Mn_{0.5}O_2$ powder quickly to the glove box to avoid adsorption of moisture. A series of Sn doping samples of $NaNi_{0.5}Mn_{0.5}Sn_xO_2$ (x = 0.01, 0.03 and 0.05) were prepared via solid-phase reaction by grinding SnO_2 powder with the solid precursor and then calcined in the same condition. Thereinto, 3 wt% Sn-doped sample indicated the mass of SnO_2 is 3% of that of the precursor.

Materials characterization: The X-ray diffractometer (XRD) patterns were obtained in a reflection mode from 10 ° to 80 ° and the scanning speed was 8 °/min using a Bruker Inc. (Germany) AXS D8 ADVANCE diffractometer (XRD, Cu Kα, 40 kV, 20 mA). The morphologies of the materials were tested by a scanning electron microscope (SEM, JEOL JEM-700F). The microstructure images and energy dispersive spectrum (EDS) analysis were obtained by high resolution transmission electron microscopy (HRTEM, FEI Tecnai G2 F20). The X-ray photoelectron spectra (XPS) of samples were recorded on a Perkin-Elmer PHI 5000C ESCA, Mg Kα, 1253.6 eV. The binding energies of all the elements were corrected regarding carbon (284.6 eV).

Electrochemical measurements: A 2032-coin cell is assembled in a glove box (H_2O, O_2 < 0.1 ppm, argon atmosphere) to evaluate the half-cell electrochemical performance of the electrode. 2025 cell was used to assemble full cells, in which hard carbon was anode and $NaNMSn_{0.03}O$ was cathode. The cathode was obtained by uniformly coating active material, carbon black and poly (vinyl difluoride) (PVDF, Aldrich) adhesive in a ratio

of 8:1:1 by weight on aluminum foil. The anode was coating on copper foil after uniformly stirring hard carbon, carbon black and sodium carboxymethylcellulose (CMC) in a ratio of 8:1:1 by weight. The resulting electrode sheet was then dried 12 h at 120°C. In the whole study, the areal density of the cathode and anode were 1.98 and 1.04 mg/cm^2, respectively. The electrolyte used in battery assembly is a 1 M $NaClO_4$ solution formulated according to 1:1 ethylene (EC) and diethyl carbonate (DEC). Pure sodium tablets were the anode material for half cells and glass fiber (GF/D) was separator. The charge-discharge test was performed in a Land system CT-2001A at 0.1 C and a constant temperature of 25°C from 2.0 V to 4.2 V for the half cell and from 1.5 V to 4.0 V, 4.05 V, 4.1 V, 4.2 V for the full cell. Cyclic voltammetry (CV) tests were executed by an electrochemical workstation CHI 660E at a scan rate of 1 mV s^{-1}. In addition, the electrochemical impedance spectra (EIS) was tested by the same equipment in the frequency range of 1 MHz–0.01 Hz.

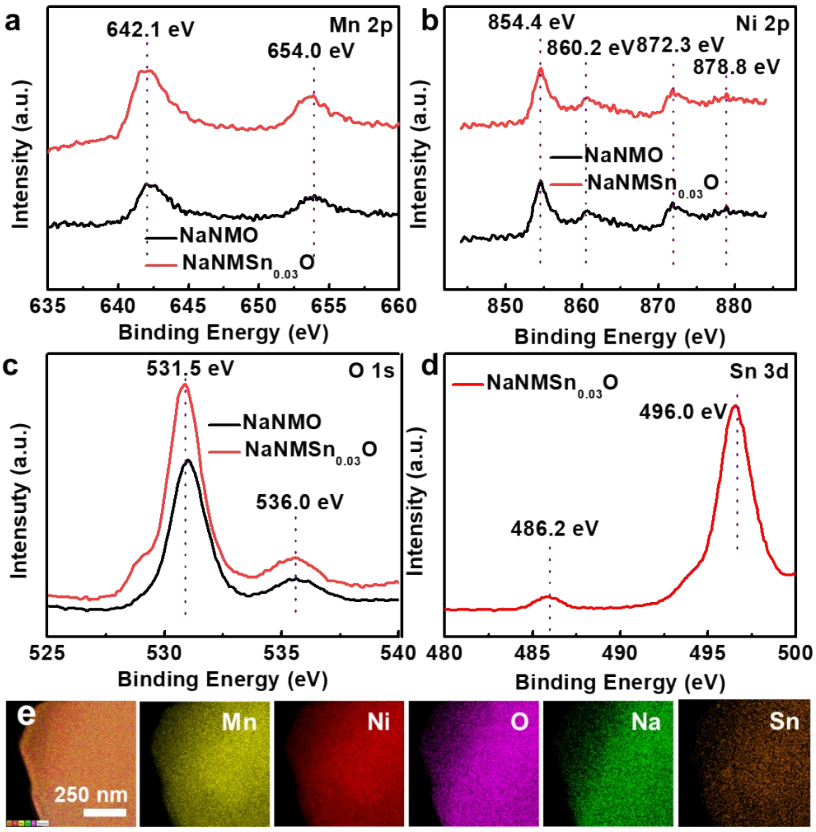

Fig. S1 XPS spectra of the oxides before and after Sn doping and elements mapping images. (a) Mn 2p, (b) Ni 2p, (c) O 1s, (d) Sn 3d, (e) HRTEM mapping of O3-$NaNMSn_{0.03}O$.

Fig. S1a shows two peaks at 654.0 eV and 642.1 eV belonging to the Mn $2p_{1/2}$ and Mn $2p_{3/2}$ peaks, respectively. It indicates that the main chemical state of Mn in both materials is +4. From the Ni 2p spectrum (Fig. S1b), it is known that the dominant peak at 854.4 eV indicates Ni has an oxidation state of +2. In the O1s spectrum (Fig. S1c), the O^{2-} anion has two features of the crystalline structure and one weakly absorbing surface specie. Obviously, the dominant position is 529.4 eV, attributed to the lattice oxygen. Another smaller peak at a higher binding energy of 531.4 eV is from the surface of active oxygen or adsorbed impurities such as Na_2CO_3. In Fig. S1d, two peaks of Sn $3d_{5/2}$ and Sn $3d_{3/2}$ located at 486.2 eV and 496.0 eV, respectively, match with the Sn^{4+} binding energy. This proves that Sn is successfully doped in the bulk material and the main chemical state of Sn in the doping material is +4.

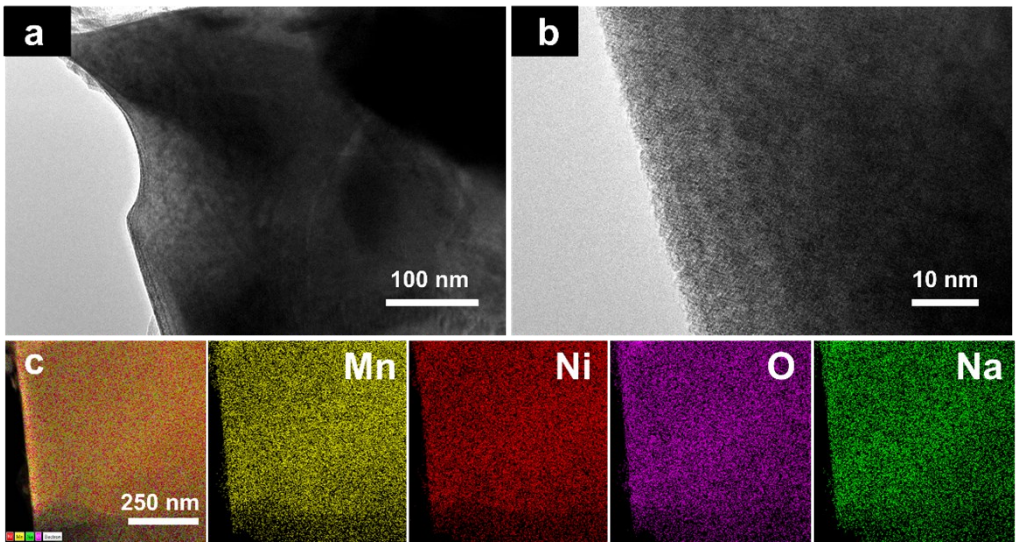

Fig. S2 HRTEM images (a) and (b) and mapping images (c) of NaNMO.

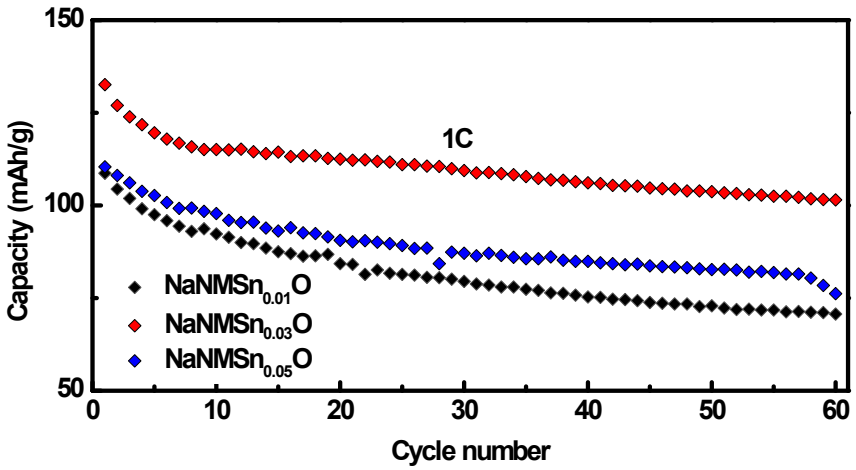

Fig. S3 Cycling performance of $NaNMSn_xO$ (x=0.01, 0.03, 0.05) materials at 1C vs. Na/Na^+.

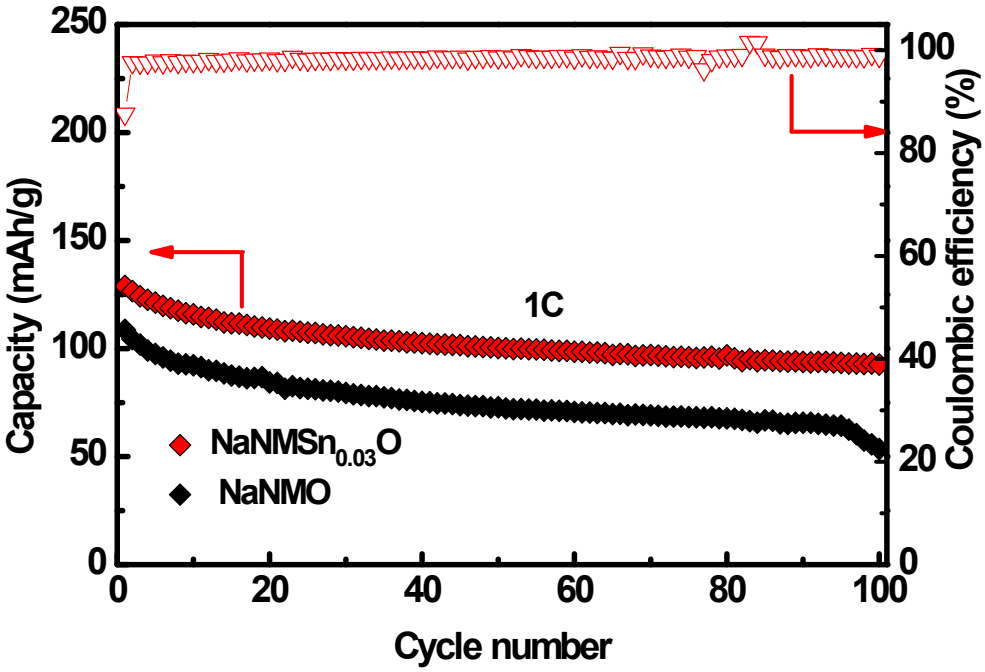

Fig. S4 The comparison of cycling performance between NaNMO and $NaNMSn_{0.03}O$ at 1C vs. Na/Na^+.

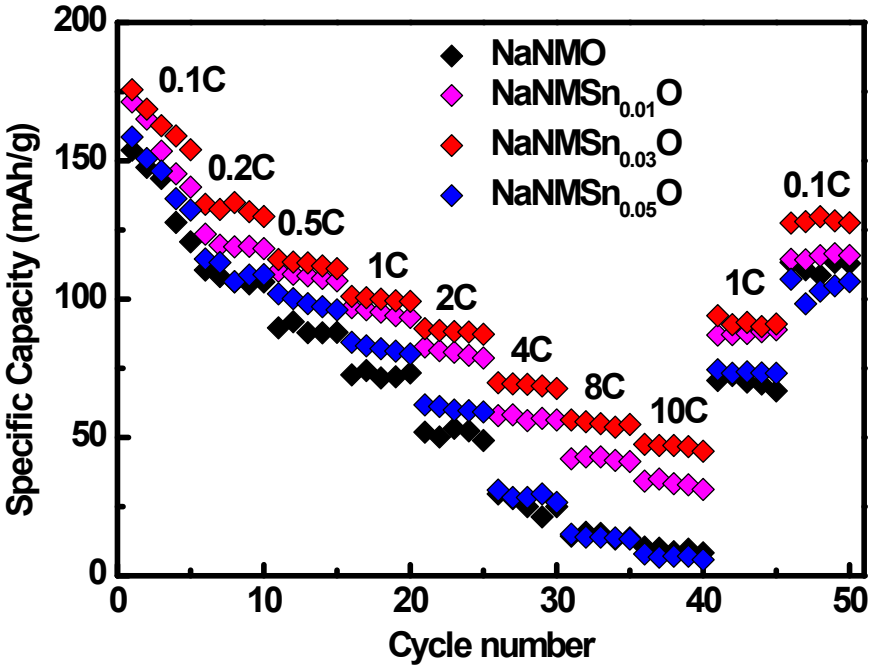

Fig. S5 Rate capability of $NaNMSn_xO$ (x=0, 0.01, 0.03, 0.05) vs. Na/Na^+.

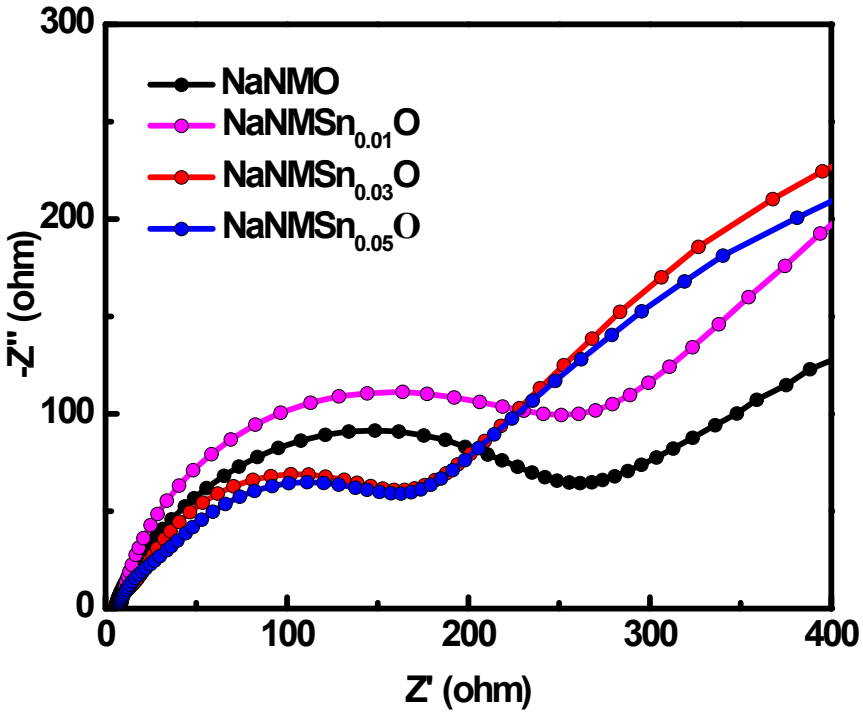

Fig. S6 Electrochemical impedance spectra of $NaNMSn_xO$ (x=0, 0.01, 0.03, 0.05) before cycling.

Generally, the EIS spectra is divided into two parts: one is the semicircle at high frequency indicating the resistance of the lithium ions through the interfacial film; the other is the slope located at low frequency indicating the process of lithium ions diffusing in the bulk material. According to the EIS results, diffusion coefficient of Na^+ can be calculated by the equation below:

$$D = 0.5\left(\frac{RT}{An^2F^2\sigma_W C_0}\right)^2 \quad (1)$$

$$Z' = R_s + R_{ct} + \sigma_w \omega^{-0.5} \quad (2)$$

As shown in Equation (1), R is the ideal gas constant; T represents the absolute thermodynamic temperature; A is the surface area of electrodes (1.77 cm^2 in this study); n is the number of electrons transferring during cycling (1 in this cathode); F represents the Ferrari constant; σ_W means the Weberge factor related to Z' (Equation (2)); C_0 is the

concentration of Na^+ per unit cell (4.61×10^{-3} mol cm^{-3} in this cathode).

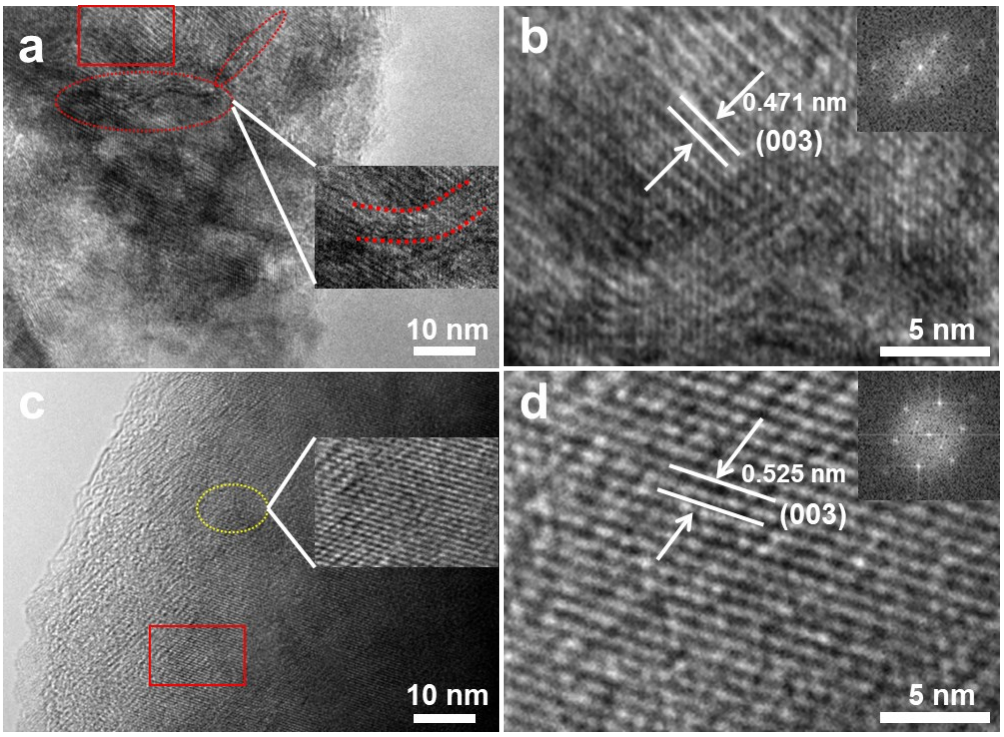

Fig. S7 HRTEM images of the materials after cycled: (a) NaNMO after 100 cycles at 1 C, (b) the selected region of (a), (c) $NaNMSn_{0.03}O$ after 100 cycles at 1 C, (d) the selected region of (c).

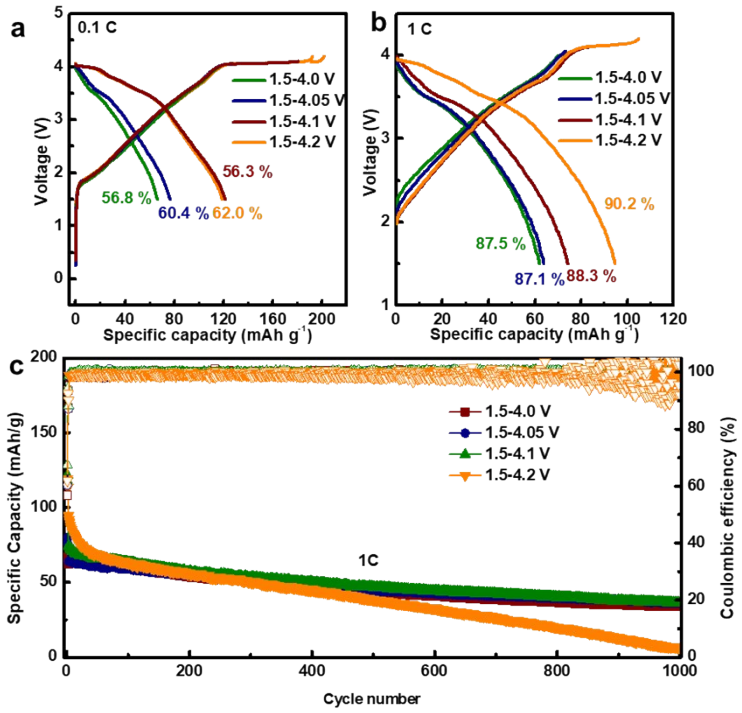

Fig. S8 Electrochemical properties of full cell at different voltage ranges. (a) First charge/discharge curves of four cut-off voltages at 0.1C. (b) First charge/discharge curves of four cut-off voltages at 1C. (c) Cycling performance at 1C.

The high cut-off voltage has been optimized because the O3-P3 phase transition highly related to electrochemical performances appears over 4.0 V during the charging process. That means the O3-P3 phase transition is mainly related to the high cut-off voltage rather than the low voltage. Different high cut-off voltage will influence the length of plateau at 4.0 V, namely the degree of phase transition, and further effect the performance. Therefore, it is necessary and reasonable to optimize the high cut-off potential.

The reason for choosing 1.5V for the low voltage is due to the potential difference between the hard carbon and the lithium metal. For the half cell, the anode is metal sodium, which is always chosen as reference electrode to confirm the potential of active material. However, the anode used in full cell is hard carbon, and there is a potential difference with sodium metal. So, the two kinds of cells are always selected different voltage range, even the cathode material is the same. Moreover, it is verified there is a 0.5 V average potential difference between the metal sodium and hard carbon,[1] which means the voltage range has to reduce at some extent when the anode changed from metal Na to hard carbon.

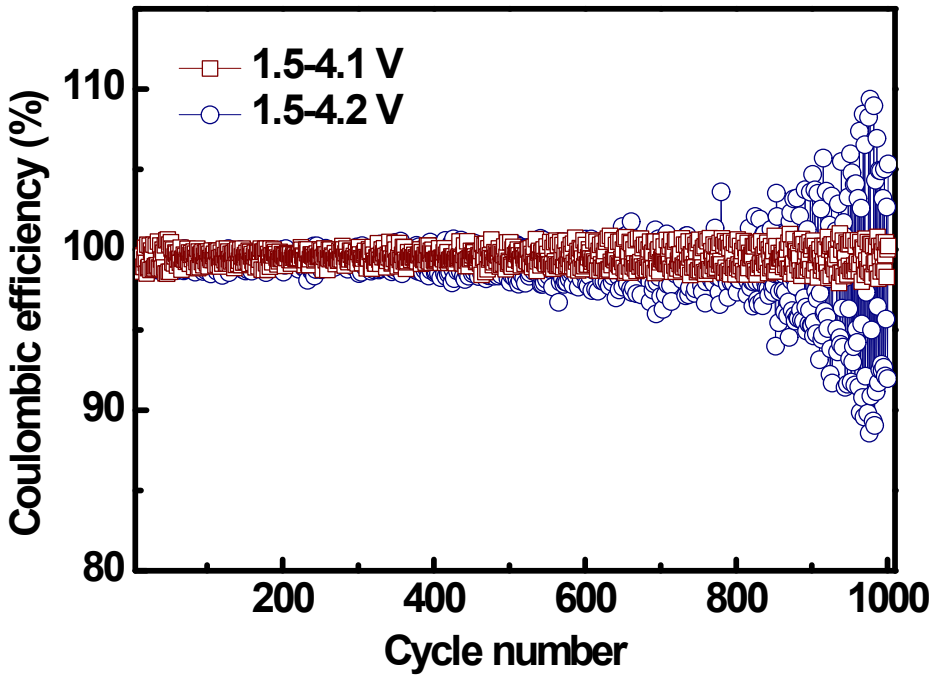

Fig. S9 The comparison of coulombic efficiency in cycling performance between 1.5-4.1 and 1.5-4.2 V at 1C.

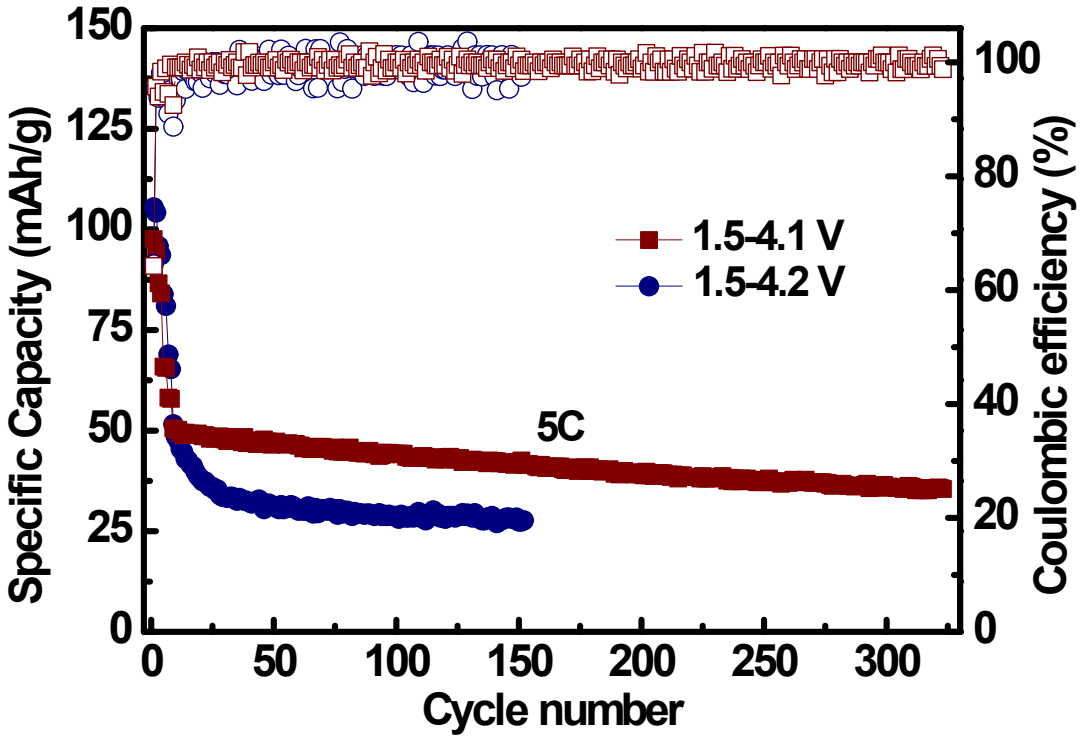

Fig. S10 Cycling performance of two cut-off voltages at 5 C.

Table S1 The crystallographic parameters of the samples obtained by using the Jade 6 software.

Sample	a(b)/Å	c/Å	c/a
NaNMO	2.9471	15.8395	5.3746
$NaNMSn_{0.01}O$	2.9504	15.9162	5.3945
$NaNMSn_{0.03}O$	2.9547	15.9394	5.3946
$NaNMSn_{0.05}O$	2.9568	15.9429	5.3919

Table S2 Electrochemical properties comparisons of previous O3-type cathode materials.

Material	Specific capacity (mAh/g)	Capacity retention of half cell (%)	Capacity retention of full cell (%)	References
O3-$Na[Li_{0.05}(Ni_{0.25}Fe_{0.25}Mn_{0.5})_{0.95}]O_2$	180.1 (0.1C)	Half cell 89.6 (0.2C, 20 cycles)	Full cell 76 (0.5C, 200 cycles)	2
O3-$Na[Li_{0.05}Mn_{0.5}Ni_{0.3}Cu_{0.1}Mg_{0.05}]O_2$	172 (0.1C)	Half cell 81.6 (1C, 400 cycles)	Full cell ~59 (0.5C, 100 cycles)	3
(P2+O3)-$Na_{0.66}Li_{0.18}Mn_{0.71}Ni_{0.21}Co_{0.08}O_{2+\delta}$	200 (0.1C)	Half cell 84 (0.2C, 50 cycles)	-	4
$Na[Ni_{0.61}Co_{0.12}Mn_{0.27}]O_2$	160 (0.1C)	Half cell 80 (0.5C, 100 cycles)	-	5
$NaNi_{0.45}Cu_{0.05}Mn_{0.4}Ti_{0.1}O_2$	124 (0.1C)	Half cell 70.2 (1C, 500 cycles)	-	6
$NaNi_{0.5}Mn_{0.2}Ti_{0.3}O_2$	135 (0.05C)	Half cell 78 (1C, 200 cycles)	-	7
O3- $Na_{0.7}Ni_{0.35}Sn_{0.65}O_2$	64 (0.1C)	Half cell 80 (0.1C, 100 cycles)	-	8
$NaNi_{0.5}Mn_{0.5}Sn_{0.03}O_2$	**191(0.1C)**	**Half cell** **85 (0.1C, 100 cycles)**	**Full cell** **82 (5C, 150 cycles)** **53 (1C，1000 cycles)**	**This work**

References

1. M. Anji Reddy, M. Helen, A. Groß, M. Fichtner and H. Euchner, *ACS Energy Letters*, 2018, **3**, 2851-2857.
2. S.-M. Oh, S.-T. Myung, J.-Y. Hwang, B. Scrosati, K. Amine and Y.-K. Sun, *Chem. Mater.*, 2014, **26**, 6165-6171.
3. J. Deng, W.-B. Luo, X. Lu, Q. Yao, Z. Wang, H.-K. Liu, H. Zhou and S.-X. Dou, *Adv. Energy Mater.*, 2017, DOI: 10.1002/aenm.201701610, 1701610.
4. S. Guo, P. Liu, H. Yu, Y. Zhu, M. Chen, M. Ishida and H. Zhou, *Angew. Chem., Int. Ed.* , 2015, **54**, 5894-5899.
5. J.-Y. Hwang, S.-T. Myung, C. S. Yoon, S.-S. Kim, D. Aurbach and Y.-K. Sun, *Adv. Funct. Mater.*, 2016, **26**, 8083-8093.
6. H.-R. Yao, P.-F. Wang, Y. Gong, J. Zhang, X. Yu, L. Gu, C. OuYang, Y.-X. Yin, E. Hu, X.-Q. Yang, E. Stavitski, Y.-G. Guo and L.-J. Wan, *J. Am. Chem. Soc.*, 2017, **139**, 8440-8443.
7. P. F. Wang, H. R. Yao, X. Y. Liu, J. N. Zhang, L. Gu, X. Q. Yu, Y. X. Yin and Y. G. Guo, *Adv. Mater.*, 2017, **29**, 1700210.
8. P. F. Wang, H. Xin, T. T. Zuo, Q. Li, X. Yang, Y. X. Yin, X. Gao, X. Yu and Y. G. Guo, *Angew. Chem., Int. Ed.* , 2018, **57**, 8178-8183.